7

Fictive temperature measurements in silica-based optical fibers and its application to Rayleigh loss reduction

Matthieu Lancry[1], Elise Régnier[2] and Bertrand Poumellec[1]
(1) Institut de Chimie Moléculaire et des Matériaux d'Orsay, Laboratoire de Physico-chimie de l'Etat Solide, UMR CNRS-UPS 8182, Université Paris Sud 11, Bâtiment 410, 91405 Orsay, France
(2) Draka Communications, Centre Data 4, Route de Nozay, 91460 Marcoussis, France

1. Introduction

For many applications, silica is the preferred material, providing excellent physical and chemical properties such as optical transparency from IR to UV range, a low thermal expansion coefficient, and a high resistance to laser induced damage. Silica-based glasses thus provide the backbone for many of today's rapidly expanding photonics applications across fields such as optical telecommunications, electronics, sensor technologies, medical applications, and materials processing.
Thus, numerous elaboration methods are used to produce v-silica-based devices. For example, the technique of vapor phase deposition i.e. Axial Deposition (VAD), Outside Vapor Deposition (OVD), Modified Chemical Vapor Deposition (MCVD), Plasma Enhanced Chemical Vapor Deposition (PECVD) is common in the fabrication of most standard telecommunication silica-based fibers or planar waveguides (Miller and Chynoweth 1979). Furthermore, other processes including sol-gel synthesis (Simmons-Potter, Potter Jr et al. 1996) or conventional melting of raw materials are routinely used to manufacture optical fibers. As a result of this large variety of elaboration processes, all the SiO_2-based glasses are different in terms of chemical composition and structural disorder (Hosono, Ikuta et al. 2001). One way to characterize the glass structural disorder is to determine the fictive temperature T_f.
As described in section 2, it is well known that the fictive temperature is linked to various glass properties such as density (Bruckner 1970; Agarwal and Tomozawa 1997), mechanical fatigue resistance (Bruckner 1970; Agarwal and Tomozawa 1997) or Rayleigh scattering loss (Saito, Kakiuchida et al. 1998). From optical fiber manufacturing point of view, monitoring the fictive temperature is thus a quick and reliable way to optimize the manufacturing process in order to reduce the Rayleigh scattering loss which is the major source of loss in telecommunication optical fibers. For a single mode telecommunication fiber, this corresponds to 90% loss at 1310nm and 80% at 1550nm (e.g. 0.16dB/km for a total of 0.19dB/km).

As recently reported in several papers (Agarwal, Davis et al. 1995; Champagnon, Chemarin et al. 1998; Le Parc 2002; Helander 2004; Koike, Ryu et al. 2005), the fictive temperature T_f of silica based glasses can be determined easily and in a reliable manner by Fourier Transform Infra-Red spectroscopy (FTIR) or Raman scattering spectroscopy. In these methods, scientists use an empirical relation that exists between the wavenumber, width or intensity of silica structural bands and the fictive temperature. Section 3 provides an overview of these methods.
However, one problem is that the features of the silica bands (position, intensity and width) vary not only with T_f but also with the elaboration process and the material composition (Agarwal and Tomozawa 1995; Kim, Tomozawa et al. 2001; Lancry, Flammer et al. 2007; Lancry, Flammer et al. 2007). This is an issue as the chemical composition of a fiber is not constant throughout its cross section but varies for designing the desired refractive index profile for a targeted application e.g. Single Mode Fiber (SMF), Multi-Mode Fiber (MMF), Pure Silica Core Fiber (PSCF), Dispersion Compensating Fiber (DCF), Dispersion Shifted Fiber (DSF). Thus, calibration curves between T_f and the IR band peak characteristics (position, intensity, width) are needed for each material composition (F, P, Ge…). In section 4, we will present an overview of all calibration curves found in the literature together with the method to realize such calibration curves.
An other important parameter that has to be taken into account is that, in general, a glass sample can exhibit different fictive temperatures at its surface and in bulk. This situation can occur, for example, when a glass is rapidly cooled from the liquid state, as it is done in fiber production. In this case, a higher T_f is expected at the fiber surface than in the bulk due to a faster cooling rate at the surface (Peng, Agarwal et al. 1997; Lancry, Flammer et al. 2007). One objective of section 5 is to examine this phenomenon in conventional optical fibers.

Minimizing the optical losses in fibers is a recurrent target for fiber manufacturers. In literature, two approaches have been proposed to reduce Rayleigh scattering loss in silica-based fibers via a reduction of T_f. Indeed, we can optimize the core and/or cladding chemical compositions (Kakiuchida, Sekiya et al. ; Tajima, Ohashi et al. 1992; Lines 1994; Saito and Ikushima 1998; Saito, Kakiuchida et al. 1998; Tsujikawa, Tajima et al. 2000; Kakiuchida, Saito et al. 2002; Saito and Ikushima 2002; Kakiuchida, Saito et al. 2003; Saito, Yamaguchi et al. 2004), or optimize the thermal conditions of the fiber drawing (Todoroki and Sakaguchi 1997; Sakaguchi and Todoroki 1998; Sakaguchi 2000; Tsujikawa, Tajima et al. 2000; Tsujikawa, Tajima et al. 2005). These two approaches are discussed in section 6.

This paper will thus give an overview of methods to measure the fictive temperature in silica-based optical fibers. We will first recall what is T_f in section 2. We will see that both Raman and IR spectroscopies can be used (Section 3). We will also show in section 4 that measuring T_f f in optical fibers requires taking many corrections into account. Section 5 will thus give some examples of T_f profiles measured in optical fibers manufactured in different conditions. Finally, section 6 will present two approaches to reduce Rayleigh scattering loss in silica-based fibers via a reduction of T_f.

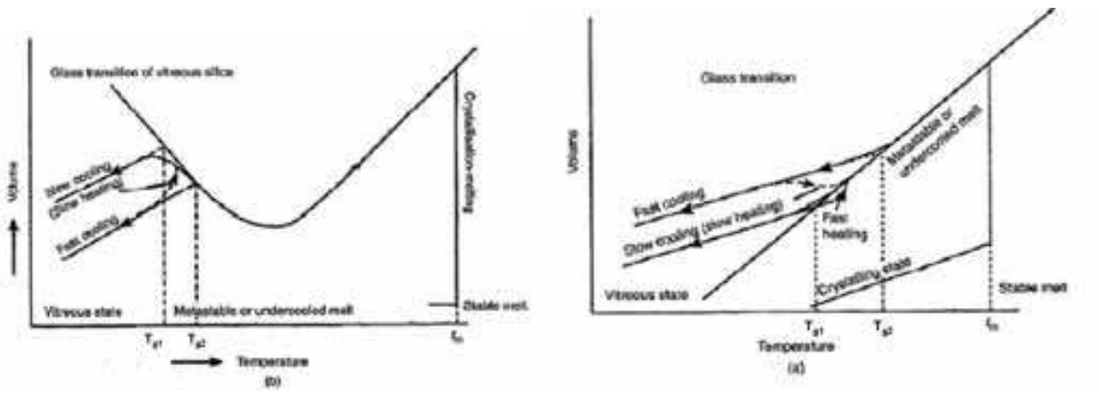

Fig. 1. Schematic diagram of specific volume-temperature relations for a) a normal glass and b) silica glass in the anomalous region (Bruckner 1970).

2. What is the fictive temperature T_f?

2.1 Definition

Glass is not merely a super-cooled liquid. The volume-temperature diagram shown in Fig. 1a illustrates this distinction. When a liquid is cooled, it crystallizes at or slightly below the melting point. If there are not enough crystal nuclei or if the viscosity is too high to allow sufficient crystallization rates, under-cooling of the liquid can occur. However, in the case of a glass, the viscosity of the liquid rapidly increases with decreasing temperature, and atomic rearrangement slows down more than would be typical for the super-cooled liquid. These observations result in the deviation from the metastable equilibrium curve as it can be seen in Fig. 1a. This change in slope is characteristic of a glass. The cooling rate determines the knee position when the deviation (from the extrapolated liquid curve) begins to occur. Slower cooling, for instance, results in a smaller deviation from the extrapolated liquid curve. Figure 1 shows that the point of intersection of the two slopes defines a transformation point i.e. glass-transition temperature (T_g), which depends on the cooling rate. Practical limitation on cooling rate defines the transformation range [T_{g1}-T_{g2}] in which the cooling rate can affect the structure-sensitive properties such as density or refractive index. The structure, which is frozen-in during the glass transformation, persists at all lower temperatures. Thus, a glass has a configurational temperature or fictive temperature that may differ from its T_g. **The fictive temperature is the temperature at which the glass structure is frozen. It describes thus the structure of a glass and is related to the cooling rate. A fast-quenched glass will have a higher fictive temperature than a slowly cooled glass.**

	Increase in fictive temperature
Density	↑ (T< 1773 K);↓ (T>1773K) [Bruckner 1970; Fraser 1968; Shackelford, Masaryl et al. 1970; Zarzycki 1982; Hong 2003]
Refractive index	↑ [Bruckner 1970]
Viscosity	↓ [Hetherington 1964; Hong 2003]
Thermal expansion α	↑ [Bruckner 1970]
Etch rate	↑ [Agarwal 1997]
Water diffusion	↓ [Roberts 1966]
Compressibility	↓ [Fraser 1968]
Shear modulus	↓ [Fraser 1968]
Young's modulus	↑ [Fraser 1968]
Rayleigh scattering	↑ [Pinnow, Candau et al. 1968; Pinnow, Candau et al. 1968; Lines 1984; Sakaguchi and Todoroki 1998; Kakiuchida, Saito et al. 2003; Tsujikawa, Tajima et al. 2005; Le Parc 2002, Champagnon 2000]

Table 1. Qualitative behavior of the effect of fictive temperature increase on silica glass structure and properties (1273K < T < 1873K). Adapted from Ref. (Agarwal and Tomozawa 1997).

2.2 Qualitative link between fictive temperature and properties of silica glass

Given a well defined chemical composition, silica glass can have different structures and properties depending upon its thermal history (Bruckner 1970; Agarwal, Davis et al. 1995). This is attributed to different fictive temperatures. Thus, the fictive temperature allows learning about glass properties such as density, refractive index, hardness, mechanical strength and chemical durability. In this section, the changes in various properties of silica glasses induced by thermal or mechanical processes reported in the literature are compared. These observations are summarized in Table 1 (adapted from (Agarwal and Tomozawa 1997)). The structural changes induced by modification of fictive temperature are considered in the anomalous region. This anomalous region is the range of fictive temperatures from 1273K to 1773K, where the density of silica glass increases with increasing fictive temperature (Fraser 1968; Bruckner 1970; Shackelford, MASARYK et al. 1970; Zarzycki 1982). This is the opposite to what happens in the other glasses. This is illustrated in Fig. 1b. In addition, Fig. 2 shows the density according to T_f for such silica glasses.

As it can be seen in Table 1, a glass with a higher fictive temperature has larger light scattering loss, larger mechanical fatigue resistance, lower viscosity and larger HF etching rate. Concerning the fiber drawing parameters, fictive temperature of fiber core and inner cladding is higher for fibers processed with a faster cooling rate, which generally corresponds to higher drawing speed or lower tension force.

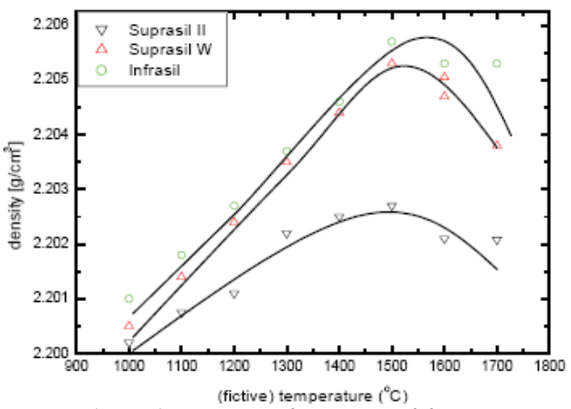

Fig. 2. Densities of various silica glasses as a function of fictive temperature (Bruckner 1971) in the anomalous region.

As this paper is dedicated to fictive temperature in optical fibers, in the following we briefly discuss the **relationship that is well known between Rayleigh scattering and fictive temperature** to estimate the intrinsic loss of silica-based fibers (Saito, Kakiuchida et al. 1998). The Rayleigh scattering coefficient R (dB/km/μm⁴) is expressed as the sum of two contributions R_ρ and R_c which are the Rayleigh scattering coefficients resulting from density fluctuations and concentration fluctuations, respectively. R_c is assumed to be independent on T_f (Martinez and Angell 2002) as it is mainly governed by dopant concentration fluctuations (e.g. polarizability differences between dopants and host material) arising from the elaboration process (e.g. higher concentration fluctuations in VAD process when compared to MCVD process (Dalle)) and the thermodynamics.

$$R_\rho = \frac{8}{3}\pi^3 n^8 p^2 k_B \beta_T T_f \tag{1}$$

R_ρ is expressed as Eq. (1), where n is the refractive index, p the average photo-elastic coefficient, T_f the fictive temperature, and β_T the isothermal compressibility for a given fictive temperature. This equation highlights the strong impact of n and T_f on the Rayleigh scattering. Equation (1) indicates that R_ρ is proportional to T_f (Pinnow, Candau et al. 1968; Pinnow, Candau et al. 1968; Lines 1984). This is indeed confirmed by experimental results that show that the Rayleigh scattering coefficient has a linear relationship with T_f in pure silica glasses and in fibers which have only density fluctuations (only R_ρ) (Sakaguchi and Todoroki 1998; Kakiuchida, Saito et al. 2003). Usually, for low dopant concentrations (case of most SMFs used in telecommunications), Rayleigh scattering is mainly caused by frozen-in density fluctuations. Figure 3 shows the relationship between the R (sum of R_ρ + R_c) value and T_f. The solid and dotted lines express the dependency in the cases of pure silica and slightly GeO_2-doped (typ. 5w %) silica glasses, respectively. In addition, the Rayleigh losses depend strongly on the wavelength (λ^{-4} dependence), that's why telecommunication transmission windows are in the NIR (Near-Infra-Red) range around the minimum attenuation window.

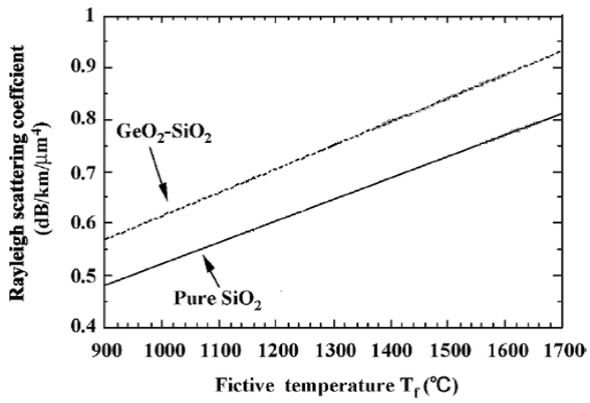

Fig. 3. Relationship between the Rayleigh scattering coefficient and T_f. Extracted from Ref. (Tsujikawa, Tajima et al. 2005).

3. Methods to determine the fictive temperature of silica glasses

3.1 Overview of methods to measure T_f

In principle, fictive temperature of a glass can be determined by measuring any glass properties. In practice, Differential Scanning Calorimetric analysis is a popular method to measure fictive temperature of vitreous materials. However this method cannot be used for silica glasses (and thus optical fibers) since they show a negligible change in specific heat around the glass transition region.

Recently, several authors have reported two methods based on IR absorption (or reflection) and Raman scattering to determine the fictive temperature of silica glass. In these methods, one uses an empirical relation between T_f and the intensity I, wavenumber σ or bandwidth $\Delta\sigma$ of silica vibrational structural bands. These correlations are summarized in Table 2 together with the interpretation and the corresponding references. Using these correlations, it is possible to determine the fictive temperature of different types of silica glasses providing that a calibration was previously established.

Method	Observations	References
Raman 440cm^{-1} band	$T_f \uparrow \Rightarrow \sigma\uparrow$ $\Delta\sigma\downarrow$	Le Parc 2002; Galeener 83
Raman D_1 (485 cm^{-1}) band D_2 (600 cm^{-1}) band	$T_f \uparrow \Rightarrow I\uparrow$	Le Parc 2002; Bates 1974; Stolen 1976; Mikkelsen 1980
Raman 800cm^{-1} band	$T_f \uparrow \Rightarrow \sigma\uparrow$	Le Parc 2002; Galeener 1983
Raman 1060/1200cm^{-1} band	$T_f \uparrow \Rightarrow \sigma\downarrow$	Le Parc 2002; Galeener 1983
FTIR, Reflectance 1120cm^{-1}	$T_f \uparrow \Rightarrow \sigma\downarrow$ $\Delta\sigma\uparrow$	Le Parc 2002; Kim 2001; Agarwal 1995; Kim 2001; Peng 1997; Hong 2003; Helander 2004
FTIR, Transmission 2260cm^{-1}	$T_f \uparrow \Rightarrow \sigma\downarrow$	Le Parc 2002; Kim 2001; Hong 2003

Table 2. Relations between fictive temperature and IR absorption and Raman scattering bands' characteristics in pure silica.

On the one hand, Raman scattering method is well adapted to realize T_f cross-section profile in optical fibers and especially in SMF as it provides a good spatial resolution (~ 1μm) (Martinet, Martinez et al. 2008). On the other hand, it has been shown that the IR absorption band located near 1120 cm^{-1}, and which corresponds to the fundamental asymmetric stretching vibration of the Si—O—Si structure, is the most sensitive to structural changes and thus to the T_f changes. This IR vibrational structural band is therefore related to the Si-O-Si bond angle (Bell, Bird et al. 1968; Galeener 1979). In addition, the determination of the peak position is much reliable using FTIR technique. Thus, in the following, the asymmetric bond-stretching vibration observed near 1120 cm^{-1} in the IR reflection spectra is monitored to determine the fictive temperature for several types of silica glasses or optical fibers. As reported in the literature, this method remains well adapted to realize T_f cross-section profiles in optical fibers (Peng, Agarwal et al. 1997; Kim and Tomozawa 2001; Kim, Tomozawa et al. 2001; Hong 2003) as the spatial resolution can be as small as 10 microns. At the opposite, IR transmission measurements are less precise (lower slope of the calibration curve between the peak position and the fictive tempertaure) and require to prepare very thin samples (thinner than 50 μm).

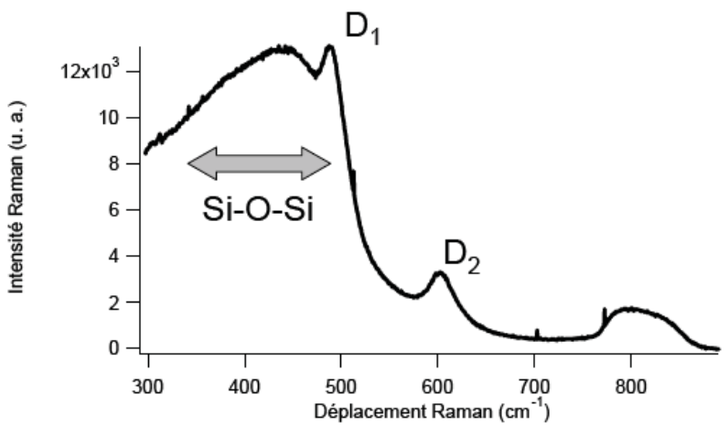

Fig. 4. Typical Raman scattering spectrum of a pure silica glass. Le parc, R. (2002)

An example of the resulting reflectance spectrum is shown in Fig. 5. This spectrum was recorded in a pure silica glass. Typically, there is a predominant IR band at 1120 cm^{-1} accompanied by a shoulder at 1200 cm^{-1}. This shoulder is due to the component which is parallel to the direction of the light propagation (the longitudinal optical, LO mode) while the main band at 1122 cm^{-1} is caused by the transversal optical (TO) mode (Bell, Bird et al. 1968; Galeener 1979).

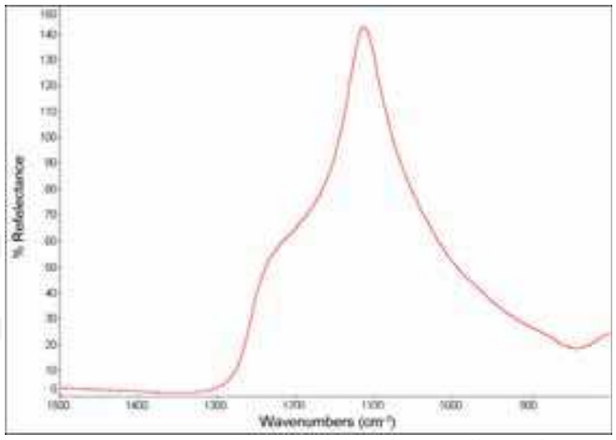

Fig. 5. Typical IR reflection spectrum of pure silica glass collected using Nexus FTIR micro-spectrometer with a maximum reflection angle of 37°.

3.2 Sample preparation, the three investigated methods

Three different methods can be used to determine the fictive temperature of SMF's (Single Mode Fiber) or MMF (Multi-Mode Fiber) cores.

3.2.1 Cleaved fiber and standard FTIR reflection measurements

The fiber was simply cleaved and then mounted vertically in epoxy resin at 90 ± 1 degrees off the horizontal direction using a V-groove metal support. Then, the mounted fiber was etched for 30s in 10% HF-10% H_2SO_4 solution to remove surface water and to reveal boundaries of the core, inner cladding and outer cladding. Figure 6 displays an optical microscope photograph of a SMF made by MCVD process. Thanks to etching we can clearly see the different parts of the fiber such as core, inner-cladding and outer-cladding. Another possibility to reveal core-cladding area will be to observe the samples between cross-polarized. Indeed, due to the chemical composition profile, relative changes in thermal expansion coefficient result in a stress and thus birefringence is radially symmetric (Bachmann, Hermann et al. 1987).

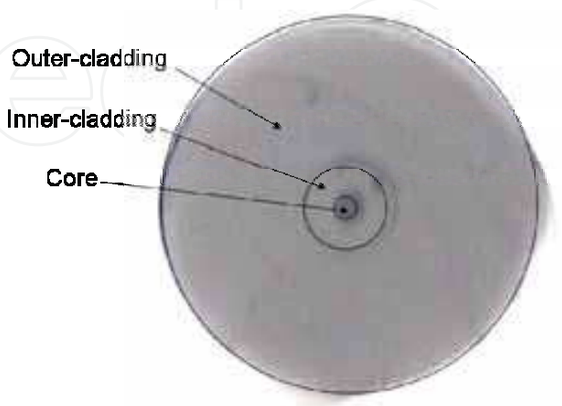

Fig. 6. Optical microscope photograph of SMF after 30 s etching in 10% HF-10% H_2SO_4 solution.

Standard FTIR: Finally, IR reflection spectra were recorded by means of FTIR spectrometer. The spatial resolution can be reduced down to 20 µm x 20 µm. Therefore this technique in well adapted to MMF measurements where the average core diameter is at least 50 microns wide. However in SMF, this results in an average value of T_f including both core and cladding. Since the beam probe size is much larger than the SMF core, it is thus necessary to perform "strong" correction, due to the cladding's impact. This degrades strongly the reproducibility of our measurements.

FTIR with FPA type detector: On the other hand, the FTIR reflection spectra can be recorded by means of a FTIR Spotlight 300 Perkin Elmer equipped with the new technology of FPA (Focal Plane Array) detector. The instrument provides 6:1 imaging on a MCT (Mercury Cadmium Telluride) detector, resulting in a nominal resolution of 8 µm x 8 µm. Using this technique, we are thus able to measure SMF's core only. However, the alignment of the probe beam on the fiber core is quite difficult since the core and pixel size are roughly similar. This can result in less reliable measurements.

Treatment	Time	Diluents
Mounting in epoxy resin	3h	
Polishing with SiC 600	few min	Water
Polishing with SiC 1200	10 min	Water
Polishing with 6 µm diamond slurry	10 min	Oil
Polishing with 1 µm diamond slurry	10 min	Oil
Polishing with 0.25 µm diamond slurry	15 min	Oil
10%HF-10%H_2SO_4 etching	30s	Water

Table 3. Samples treatments before FTIR reflection experiments: mounting, polishing and etching.

3.2.2 Blaze polished fiber and FTIR

Instead of trying to reduce the beam probe size, as shown in the previous section, in the following, the fiber is cleaved and then polished at very small angle (typ. a few degrees), in order to increase the fiber core surface area. In this view, the fibers are mounted in epoxy resin a few degrees off the horizontal direction using a thin taper plastic as a holder. This is illustrated in Fig. 7a. Next, the mounted fibers are polished horizontally to reach optical quality (λ/50). The samples are polished with a series of 600 and 1200 grid silicon carbide and then using 6µm, 1µm and 0.25µm diamond polishing powder in oil. The typical parameters are reported in Table 3. The polishing machine was configured to 100rpm. Notice that the polishing step is very important since surface roughness strongly impacts both the IR peak intensity and its position when measured in reflectance configuration. This is illustrated in Fig. 8 where the peak is shown for various surface roughnesses. Typically the peak shift (towards smaller wavenumbers) can be as high as 4 cm^{-1} when average surface roughness (RMS) increases from 0.055 to 0.27 microns (Hong 2003).

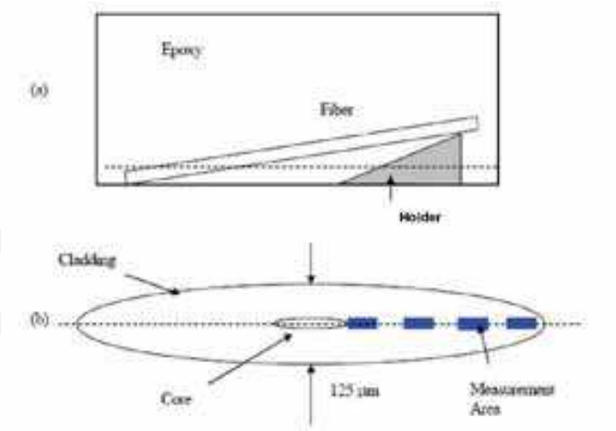

Fig. 7. Schematic diagram for the procedure to create an elongated cross-section of an optical fiber (Hong 2003). a) Mounting of the fiber in epoxy resin at an oblique angle using a thin tapered base. b) Cross-section of the fiber after polishing up to the dotted line indicated in Fig. a.

The polished fibers were subsequently etched for 30 s in 10% HF-10% H_2SO_4 solution to reveal boundaries of the core, inner-cladding and outer-cladding. Finally, the FTIR reflection spectra were recorded by means of standard FTIR spectrometer as shown in Fig. 7b. Spectra have been recorded in the 800 cm^{-1} to 2000 cm^{-1} spectral range with a spectral resolution of 4 cm^{-1} and by averaging 512 scans. The mask size was close to 8 μm x 100 μm resulting in a probe area corresponding to the SMF core only.

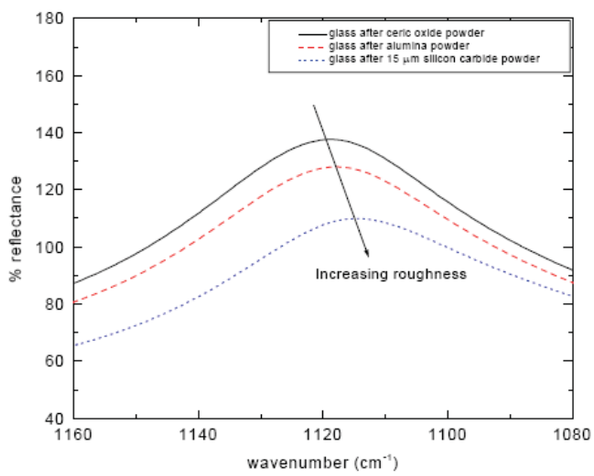

Fig. 8. Shifts in peak positions and intensity of the 1120 cm^{-1} band in IR reflection for GeO_2 doped silica glasses with different surface roughness (Hong 2003).

3.3 Experimental setup

FTIR reflectance spectra were recorded by means of either a Nexus FTIR Spectrometer (Nicolet) or a FTIR Spotlight 300 (Perkin Elmer) equipped with the new technology FPA

(Focal Plan Array) MCT (Mercury Cadmium Telluride) detector. This last instrument provides 6:1 imaging on MCT detector, resulting in nominal resolution of 8 μm. Visible images are recorded under white light LED illumination and are collected via a charge couple device CCD camera to give pictures of arbitrary size and aspect ratio. The desired regions for the IR images are selected from visual images. Typically, we need a few minutes only to perform a mapping of 1 mm^2 area. The spectra have been recorded in the 800 cm^{-1} to 2000 cm^{-1} spectral range using a spectral resolution of 4 cm^{-1}. The spectra were obtained by averaging only 32 scans (because the signal to noise ratio remains quite high using this technique). When using a standard FTIR spectrometer, spectra have been recorded in the 800 cm^{-1} to 2000 cm^{-1} spectral range with a spectral resolution of 4 cm^{-1} and by averaging 512 scans. In a general manner, the mask size can be reduced down to 20 μm x 20 μm.
Notice that the specular reflection data were collected at a fixed angle of incidence. Indeed, as shown in Fig. 9, a variation in the angle of incidence changes the IR reflection band positions (Almeida 1992; Hong 2003). Thus, the use of the same angle of incidence (i.e. 37° in our experiments) is needed for a reliable determination of fictive temperature.

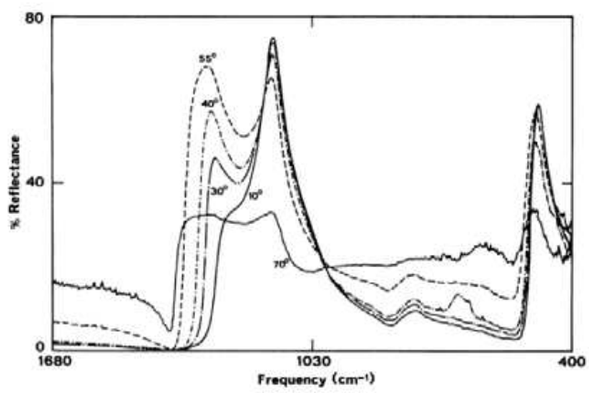

Fig. 9. Specular reflectivity spectra of vitreous silica at different angles of incidence (Almeida 1992).

3.4 Data treatment

An example of the resulting reflectance spectra is shown in Fig. 5. Typically, there is a predominant IR band at 1120 cm^{-1} accompanied by a shoulder at 1200 cm^{-1}. However, one cannot simply choose the wavenumber associated to the largest intensity of an IR band data and call it the peak position because spectral data points are only collected every 2 or 4 cm^{-1}. Indeed, lower spectral resolution results in a much higher noise in the peak determination and thus less precise fictive temperature determination. Hence, the IR peak position was determined by performing a least square polynomial fit and then calculating the minimum of the second derivative using OMNIC@Nicolet or any other fitting software. This is illustrated in Fig. 10. However, one has to be careful because firstly, the sensitivity to noise increases with increasing polynomial degree. Secondly, the choice of the discrete data points used for the fit is very crucial. For instance, if the spectral window width chosen for the fit is too large, shifting the data one step towards higher or lower wavenumber can change the peak position as much as 0.3 cm^{-1}. As the peak position shifts in wavenumber according to the probing area, it is also necessary to change data points for the fit (we cannot keep a fixed

spectral window). Thus, we choose to fix the set of 25 data points around the maximum peak position. Indeed, some interference from a shoulder around 1200 cm^{-1} might occur for larger range. Finally, by changing the set of data or the window width and recalculating the peak position, the stability of the fit is verified. Using this treatment and optimized experimental conditions, we are then able to determine the peak wavenumber with a precision around 0.1 cm^{-1}.

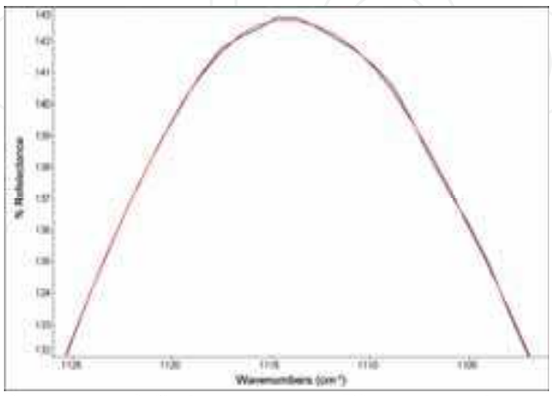

Fig. 10. Illustration of the spectral fitting process. Blue curve is a guide for eye while red curve is for the fit curve.

3.5 Typical results

To summarize, three different methods have been presented to follow the fictive temperature within either MMF or SMF core. In all cases, the 'bond-stretching' vibration mode observed near 1120 cm^{-1} in the FTIR reflection spectra was considered to determine the fictive temperature of the fiber core. Table 4 summarizes the main parameters for each case: type of sample (MMF or SMF, core or cladding), method, spent time (sample preparation + five measurements), spatial resolution, repeatability on T_f measurements (relative error) and number of scans.

For MMF core, there are no peculiar problems due to the large core size (at least 50 microns). We can simply cleave the fiber and probe the core using a standard micro-spectrometer. Typically, the relative error on T_f is lower than ± 20°C. In the case of SMF core, this is slightly more complex due to the small core size i.e. around 8 microns in diameter. From our results, the blaze polished fiber method is the most precise, straight and reliable method, at the expense of a larger time spent.

Specimen	Method	Spent time	Spatial resolution	T_f relative error	Scan times
MMF core	Cleaved	1 hour	30 µm x 30 µm	± 20°C	512
SMF core	Cleaved	1 hour	20 µm x 20 µm	± 30°C	512
SMF core	Cleaved + FPA	1 hour	8 µm x 8 µm	± 40°C	32
SMF core	Blaze polished	6 hours	8 µm x 100 µm	± 20°C	512
SMF inner-cladding	Blaze polished	6 hours	20 µm x 100 µm	± 20°C	512
SMF outer-cladding	Blaze polished	6 hours	40 µm x 100 µm	± 20°C	512

Table 4. Comparison between methods used to estimate the fictive temperature in SMF core.

4. Determination of calibration curves between the IR peak wavenumber and the fictive temperature Tf in silica-based optical fibers

Currently, the main dopants involved in optical telecommunications are, on the one hand, germanium and phosphorus to increase the refractive index, and on the other hand, fluorine to lower the index. The impact of these elements is not limited to a simple variation of refractive index. By doping silica, viscosity, chemical diffusion, absorption, non-linear index etc ... are modified.

Germanium is now the most widely used dopant in silica-based glasses. Indeed, GeO_2 is common for increasing the refractive index of silica (Kao 1983). It is usually found in concentrations ranging from 1 to 30 w%. Up to now, GeO_2 remains also the most prominent dopant to obtain highly photosensitive silica glass to UV light, allowing thus the writing of optical components such as fiber Bragg gratings (Othonos 1997).

Fluorine-doped silica glasses occurs in a variety of technological applications (Gonnet, Nouchi et al. 2007; Matthijsse, Gooijer et al. 2007; Regnier, Kuyt et al. 2008), due mainly to the beneficial changes in optical and physical properties that results from the addition of small quantities of fluorine to pure amorphous silica. Notice that in contrast to Ge and P, which are network formers, fluorine is a network modifier. For optical fiber technology, fluorine is one of only two dopants that decreases the refractive index of silica, the other being boron (Kao 1983). This has resulted in the widespread application of fluorine doping of silica to control the refractive index profile of optical fibers (Kao 1983; Matthijsse, Gooijer et al. 2007). Small contents of F (<1 wt%) have also been introduced to reduce the additional imperfection loss by allowing viscosity-matching. Note that this viscosity-matching technique can also be used with dopants like GeO2 or P2O5 (Kao 1983).

The presence of P_2O_5 reduces strongly the glass viscosity. In optical fiber manufacturing, this allows a relatively low deposition temperature. However, this also leads to a strong increase of the thermal expansion coefficient (and thus a mismatch between P-doped and P-free parts). In addition, the presence of large amounts of P_2O_5 in the core or the cladding can lead to an attenuation increase at long wavelengths (Regnier, Poumellec et al. 2005). Therefore phosphorus is rarely used at high content, and it is then rarely used alone as dopant in silica. That is why many studies on phosphorus have been made in Ge or F co-doped silica glasses (Irven, Harrison et al. 1981). F-P co-doped cladding allows bringing the cladding viscosity closer to that of the core and therefore decreases excess loss. This allows stress reduction at the core-cladding interface and thus reduction in defects and imperfections at the interfaces.

4.1 Literature survey of the calibration curves in silica-based glasses

The radial variation of T_f in optical fiber cross section has been studied recently with some divergent results (Peng, Agarwal et al. 1997; Wissuchek, Ponader et al. 1999; Kim and Tomozawa 2001; Kim, Tomozawa et al. 2001; Helander 2004). One problem is that the reflection peak position varies not only with T_f but also with the material composition (Tajima, Ohashi et al. 1992; Lines 1994; Saito and Ikushima 1998; Saito, Kakiuchida et al. 1998; Tsujikawa, Tajima et al. 2000; Saito and Ikushima 2002; Saito, Yamaguchi et al. 2004). This is an issue as an optical fiber has different compositions in the core and in the cladding surrounding the core. Thus, calibration curves between T_f and the IR band peak position

must be determined for each material composition and especially for Ge, P and F-doped silica.
We have thus reported in Table 5, most of the calibration curves reported in the scientific literature for various silica-based glasses. We have also displayed the experimental temperature range and the corresponding references. The equations displayed in Table 5 are in the form: $\sigma_{1120} = A - B.T_f$, where σ (cm^{-1}) is the peak wavenumber (or spectral position) of the Si-O-Si asymmetric stretching band measured in reflectance and T_f (K) is the fictive temperature of the silica glass.

Materials	Calibration equation $\sigma_{1120} = A - B.T_f$	Experimental temperature range (K)	Reference
Doped silica			
Ge-doped preform core 3.6 w% 4.7 w % 5.7 w% 6.3 w %	 1130.494 - 0.00709. T_f 1129.325 - 0.00678. T_f 1128.412 - 0.00681. T_f 1127.855 - 0.00687. T_f	1150-1500	Hong 2003 Hong 2004
5 w% Ge-doped bulk	1128.3197 - 0.00673. T_f	1150-1500	
5.3 w% Ge-doped bulk	1128.0034 - 0.00569. T_f	1150-1500	
F-doped Inner cladding	1131.088 - 0.00583. T_f	1150-1600	Kim 2001
Pure silica			
Silica bulk glasses (e.g. infrasil, suprasil 2, suprasil W2, …)	1132.01 - 0.00686. T_f	1150-1500	Hong 2003 Agarwal 1995
Silica bulk glass	1131 - 0.0069. T_f	1350-1750	Le Parc 2002
CVD silica bulk cladding	1131.500 - 0.00742. T_f	1250-1550	Hong 2003 Tomozawa 2005
CVD silica fiber outer-cladding	1132.501 - 0.00669. T_f	1150-1600	Kim 2001 Hong 2003

Table 5. Calibration curves (between T_f and 1120cm^{-1} peak wavenumber measured in reflection) reported in the scientific literature for various silica glasses and optical fibers.

It is worth noticing that no significant difference was found between the different kinds of pure silica glasses i.e. Infrasil, Suprasil 2, Suprasil W2. In contrast, doped silica exhibit strongly different calibration curves, especially for the A coefficient. Unfortunately, the fictive temperature of highly Ge-doped glasses (> 6.7 w % in GeO_2) cannot be estimated reliably due to the lack of calibration curves (Kim, Tomozawa et al. 2001; Hong 2003; Hong, Ryu et al. 2004). Thus, we determine in next section a complete set of calibration curves for germanosilicate glasses for Ge from 1w% to 30w%. Using these curves, we will be able to determine the T_f of Ge-doped glasses whatever the Ge-content may be (between 1 and 30 wt%).

4.2 Determination of calibration curves in Ge-doped silica

4.2.1 Samples preparation and treatments

The specific case of strongly Ge-doped silica has never been reported to our knowledge because it is impossible to cut a highly Ge-doped preform rod into slices without breaking it because of the high level of stress. We have thus circumvented this tricky point by using a graded index preform and by reducing the preform diameter by a factor of 100. A graded index preform with a Ge-doping level up to 30w% was thus stretched into "capillaries"; which are in fact full rods corresponding to the initial preform composition but with a smaller diameter. This allows cutting the capillaries into slices while keeping the spatial resolution to perform many calibration curves for various Ge contents in the same sample. The capillaries were then cut to the desired length to realize the calibration standards. In order to achieve different uniform fictive temperatures in the calibration standards, the samples were held at various temperatures for long time periods, long enough (up to a few 100s hours) to ensure full structural relaxation of the whole preform diameter (i.e. outer-cladding, tube and core). The typical temperatures selected were between 1223 K and 1523 K with an uncertainty around ±2 K (furnace uncertainty). Previous data on bulk silica glass (Sakaguchi and Todoroki 1999; Kim, Tomozawa et al. 2001; Hong 2003) were used to determine appropriate heat treatment times needed to obtain a complete structural relaxation at each heat-treatment temperature. Typical heat-time of bulk silica glasses are shown in Table 6. After heating treatment, these samples were rapidly (< 1s) quenched in water to fix the uniform fictive temperature at the heating temperature (since the relaxation times have been estimated to be a few 100's at these temperatures (Sakaguchi and Todoroki 1999)). Then, the capillaries were polished with a series of 600 and 1200 grid silicon carbide and then to an optically smooth finish with 6µm, 1µm and 0.25µm diamond polishing powder in oil. The polishing machine was configured to 100rpm. Finally, the IR reflection spectra were measured as a function of the radial position (and thus the Ge content) within capillaries.

Temperature	Ge-doped Core	F-doped inner cladding	Pure silica outer cladding
1223K	134h	8h	
1273K	32h	3h	200h
1323K	29h	2h	120h
1373K	8h	1h	66h
1423K	5h	1h	45h
1473K	2h	1h	15h
1523K	1h	1h	3h
1573K			1h

Table 6. Heating treatment conditions of optical fiber capillaries.

4.2.2 Examples of IR reflection spectra in Ge-doped silica

An example of the resulting reflectance spectra is shown in Fig. 11. These spectra were recorded at various locations corresponding to various Ge content of a GI-MMF capillary. We have shown four spectra corresponding to silica outer-cladding (i.e. natural undoped silica), and 5 w%, 15 w% and 25 w% Ge-doped cores. Typically, there is a predominant IR

band at 1120 cm^{-1} accompanied by a shoulder at 1200 cm^{-1}. We can see that the higher is the Ge concentration the lower the wavenumber of TO mode related peak.

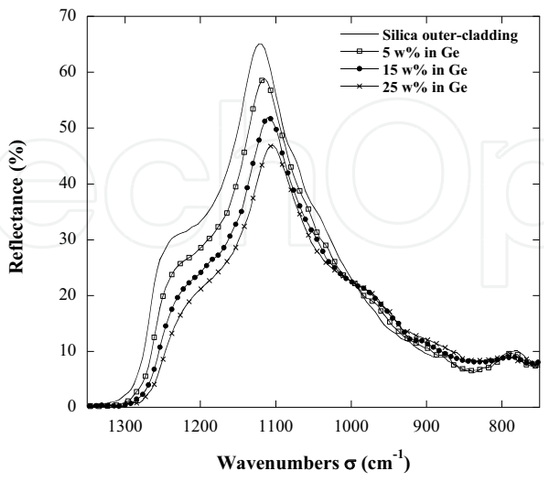

Fig. 11. Typical reflectance spectra corresponding to various location and thus Ge content for the GI-MMF capillary.

4.2.3 2D distribution of the IR peak wavenumber in GI-MMF capillaries annealed at various temperature

Figure 12 displays the 2D distribution of the peak wavenumber σ related to the Si-O-Si asymmetric stretching band recorded in reflection. The circle (black solid line) corresponds to the core part within the capillary. In this figure, the darker the color, the higher the peak wavenumber σ (in cm^{-1}). These results indicate that the concentric distribution of σ is quite constant for a fixed radial position r (constant along a circle) whereas it changes strongly according to the radial position r. In the following, we will extract the radial profiles from these data.

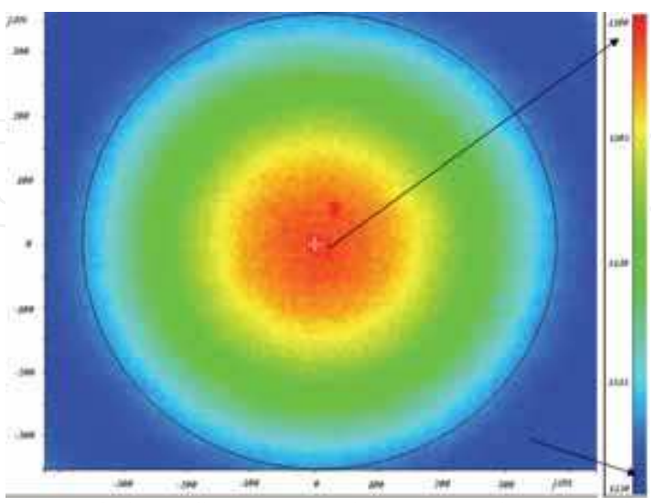

Fig. 12. 2D distribution of the reflectance peak wavenumber σ in the core of the MMF capillaries cross section

4.2.4 Determination of calibration curves: influence of the Ge concentration

In this part, we will extract the data obtained above in order to determine calibration curves between the fictive temperature and the IR reflection peak wavenumber σ for Ge concentrations up to 30 w %. Firstly, we have assumed that the drawing around 2300 K of the preform into rods did not change the germanium concentration profile since it has been shown that it did not change significantly the refractive index profile [20] when compared to our spatial resolution. We have thus converted the radial position r into Ge concentration in the GI-MMF rods using the well-known GI-MMF concentration profile in preform. Now, we are able to follow the evolution of the peak wavenumber according to the fictive temperature T_f (also called the calibration curves or master curves) for various Ge contents.
Figure 13 displays several of these calibration curves for pure silica glass and for various GeO_2 contents from 5 w % to 30w%. In this figure, the symbols are for experimental data while the full lines correspond to best fits of the data using a linear law. The least square regression analysis reveals the following relationship between fictive temperature and IR peak position: $\sigma(Ge, T_f) = A(Ge) - B(Ge) \times T_f$, where the coefficients A and B could depend on the Ge content. Based on those calibration curves, the fictive temperatures of Ge-doped (up to 30 w %) optical fibers can be estimated once the composition of the core is known.
In the following, we will investigate more precisely the effect of the Ge content on the calibration curves parameters: i.e. the ordinate at the origin (coefficient A in cm^{-1}) and the slope B (in $cm^{-1}\ K^{-1}$). We have thus extracted these values from the above linear regressions for various Ge concentrations up to 30 w%. Figures 14 and 15 display the evolution of these two parameters according to the Ge concentration together with the error bars. As it can be seen, the coefficient A follows a linear relationship with the Ge content ***(up to 30 w %)***: A = (1129.8 ± 0.1) – (0.469 ± 0.004) x [Ge]. In contrast, the slope B appears to gradually decrease with increasing Ge content. However, this decrease is not significant enough when compared to our measurements uncertainty. In the following, we will thus assume that the slope B is independent on [Ge]: B = 0.0102 ± 0.0002.

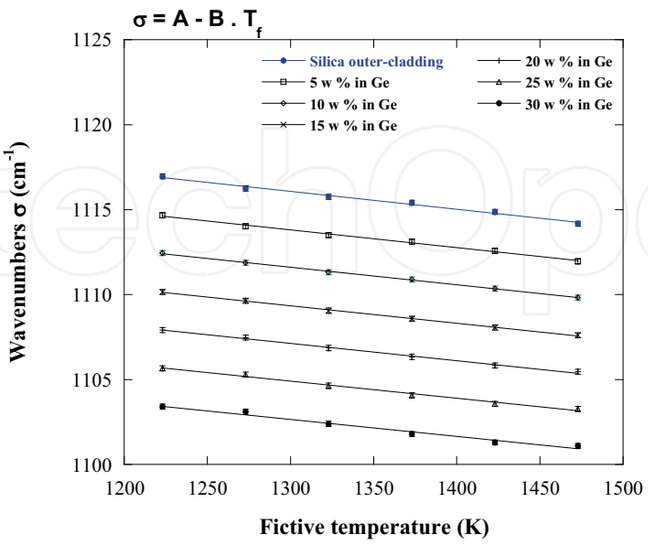

Fig. 13. The relationship between IR peak wavenumber and the fictive temperature for Ge-doped bulk silica for various Ge concentrations.

Our results are in good agreement in terms of both slope and peak position evolutions according to the Ge content when compared to those already published by Hong et al. (Hong 2003; Hong, Ryu et al. 2004) (from 3.6 w % to 6.7 w % in Ge). However, there exists a small discrepancy in the absolute values of A and B coefficients. Indeed, one can find in the literature various data (Agarwal, Davis et al. 1995; Kim, Tomozawa et al. 2001; Le Parc 2002; Hong 2003; Hong, Ryu et al. 2004) in which the slope B changes from 0.0065 to 0.0075 and A from 1131 cm^{-1} to 1132.5 cm^{-1}. There are two main explanations (not exclusive) for A variations. Firstly, a change in the maximum angle of incidence of the IR beam probe (28° for Hong measurements and 37° in our experiments) changes the IR reflection band wavenumber (Almeida 1992). Secondly, due to the significant influence of the surface roughness on the peak position (Hong 2003), the difference in the HF etching time or HF etching rate (due to the different dopant concentration) can lead to changes in the peak position.
Next the difference on the B coefficient could be due to the large difference into elaboration process: MCVD in Hong experiments, PCVD in this study. Indeed, this leads to different kind (and/or level) of "impurities" (e.g. Na, Cl, Al) or small compositional variations such as the presence of F or P. Furthermore, it is well known that a few 100's ppm (or even less) of such impurities can change A and B coefficients significantly (Tajima, Ohashi et al. 1992; Lines 1994; Saito and Ikushima 1998; Kim, Tomozawa et al. 2001).

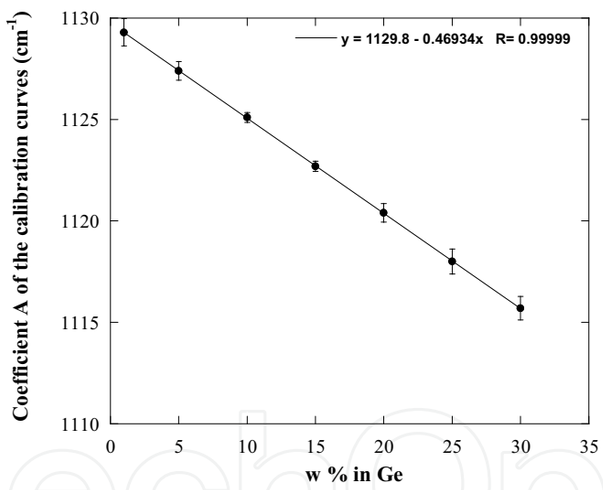

Fig. 14. Relationship between the ordinate at the origin A of the calibration curves for various Ge concentrations.

From above results, we have determined the relation (2) to estimate the fictive temperature profile from the IR peak wavenumber σ In this relation, [Ge] is the germanium content in w % in the range between 1 and 30 w %. This allows us to estimate the fictive temperature (in K) for any radial position r providing that the Ge concentration [Ge] is known.

$$T_f(r) = \frac{A(Ge) - \sigma(r)}{B} = \frac{1129.8 - 0.469.[Ge](r) - \sigma(r)}{0.0102} \quad (2)$$

Using the above reported uncertainties, we have estimated an absolute uncertainty in the fictive temperature around 4 %. This estimate is mainly due to the slope B uncertainty. In

contrast, the relative error (from one sample to another) which is independent on the calibration curves is around 1 %.

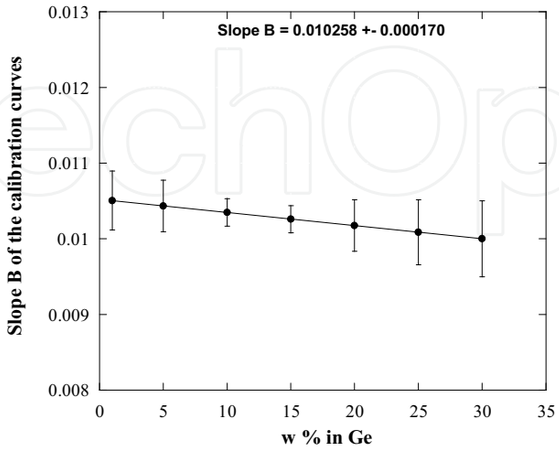

Fig. 15. Relationship between the slope B of the calibration curves for various Ge concentrations.

5. Application 1: measurements of fictive temperature distribution in multimode optical fibers

In general, a glass sample can exhibit a different fictive temperature T_f at its surface and in bulk. This situation can occur, for example, when a glass is rapidly cooled from the liquid as it is done in fiber production. In this case, a higher T_f is expected on the fiber surface than in the bulk due to a faster cooling rate at the surface (Peng, Agarwal et al. 1997; Lancry, Flammer et al. 2007; Martinet, Martinez et al. 2008). One objective of the present section is to examine this occurrence in graded index multimode optical fibers (GI-MMF) and the difficulty is that the composition changes with the radius position.

5.1 Samples

Prototype graded index multimode fiber (GI-MMF) labeled P1 was realized in typical drawing conditions (i.e. drawing speed and tension) for these experiments by Draka Communications using PCVD process. Fiber has silica outer cladding with a diameter of 125 m and a GeO_2-doped core with a diameter of 50μm. The typical refractive index profile follows a parabolic law within the core. The maximum Ge concentration of the investigated fibers is 15.00 ± 0.05 w%. The outer-cladding was made with pure silica. Next, the fiber was cleaved and mounted in epoxy resin at 90 ± 1 degrees using a V-groove metal support. The mounted fiber was then etched for 30s in 10% HF-10% H_2SO_4 solution to remove surface water and to reveal boundaries of the core, inner cladding and outer cladding. Finally, IR reflection spectra were recorded by means of the Spotlight 300 FTIR spectrometer.

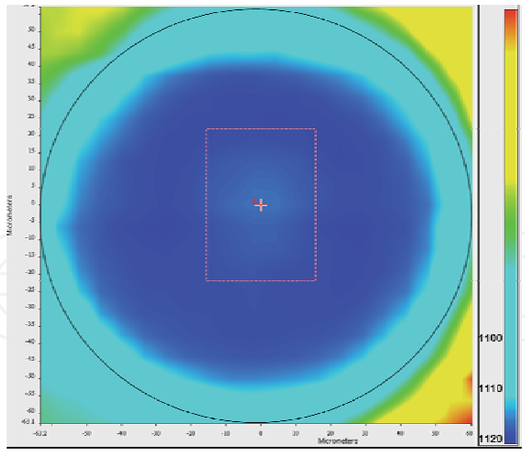

Fig. 16. 2D distribution of the reflectance peak wavenumbers σ for the GI-MMF fiber cross section.

5.2 Measurements of σ distribution in multimode optical fibers

Figure 16 displays the 2D distribution of the peak wavenumbers related to the Si-O-Si asymmetric stretching band in reflection. As it can be seen, we have added two concentric circles (solid lines) on this picture corresponding to the core and the fiber outer-diameter. Darker is the color, higher the peak wavenumber σ. These results indicate that the concentric distribution of σ is quite constant for a fixed radial position r (constant along a circle) whereas it changes according to radius value. For going further in our analysis, we extract the radial profiles from these data in the following. Figure 17 shows the evolution of σ as a function of radial position for P1 multimode optical fiber. Firstly, the peak wavenumber radial distribution is not uniform across the core. More precisely, one can observe a nearly parabolic profile within the core. This is presumably due to the effect of the Ge-doped core, the wavenumber increases from the center of the core towards the tube. Secondly, the values of σ shift towards higher wavenumber near the fiber edges (fiber surface).

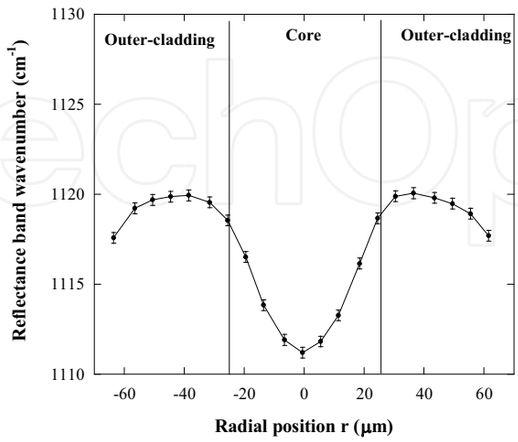

Fig. 17. Radial profile of the reflectance peak wavenumber σ for MMF cross section. Fiber was MMF made by PCVD process.

5.3 Determination of fictive temperature radial profile in MMF

As explained in the introduction, it is well known that the reflection peak position varies not only with T_f but also with the material composition (e.g. core/cladding). As in the case of MMF, the Ge concentration [Ge] in the core is not constant but follows a parabolic law, we need to use our calibration curves between T_f and σ for various Ge content in order to correct the peak wavenumber radial profile for determining the T_f profile. Therefore, we have calculated the Germanium concentration radial profile in the MMF's for converting the profile σ = f(r) into fictive temperature profile using the relation (1). Figure 18 shows the estimated fictive temperature distribution on the cross section of the P1 optical fiber. Those data correspond to the IR peak wavenumber σ shown in Fig. 17. The absolute error bars in fictive temperature have been estimated from those in wavenumbers and calibration curves (see section 4). The T_f along the entire cross-section for the P1 fiber varied with radial position. Firstly, the estimated fictive temperatures at the near-surface region are ≈ 200°C higher than inside presumably due to the faster cooling. Secondly, there is an increase (≈ 150°C) of the fictive temperature from the core-cladding interface towards the center of the core (higher Ge content) which is likely due to the constrained cooling of the fiber core.

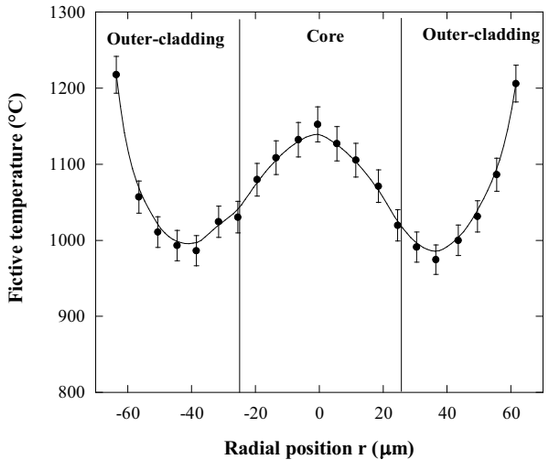

Fig. 18. Estimated fictive temperature as a function of the radial position for P1 fiber. The solid line is a guide for eyes. Fiber was MMF made by PCVD process.

5.4 Discussion

The absolute error in fictive temperature has been estimated from those in wavenumbers and due to the calibration (i.e. the calibration coefficients A and B in Equation 2). Using the above reported uncertainties, we have estimated an absolute uncertainty around 4 % in the fictive temperature which is mainly due to uncertainty on the slope B. The absolute error on the fictive temperature is thus around 40°C. Furthermore, the relative error which is independent of the calibration curves is around ± 20°C.

Now, let us discuss the reliability of the fictive temperature profile shape. In the GI-MMF, the pure silica outer-cladding had the highest viscosity while the Ge-doped core had the lowest viscosity. Typically when cooled at a constant rate, a glass with higher viscosity is expected to acquire a higher fictive temperature. Therefore, the core is expected to have 1/ a non uniform T_f due to the Ge profile (lower T_f for higher Ge content) and 2/ a lower fictive

temperature than the outer-cladding. However, in our measurements, the fictive temperature of the core is higher in the center (higher Ge content) and even higher than in the interior (e.g. from -50 to –25 μm) of the outer-cladding. This is puzzling. This can be due to the stress distribution as discussed in the next paragraph.

A problem that we could meet is the impact of the way to establish the calibration curves. Indeed we need a uniform T_f across sample cross-section but because of the different properties (e.g viscosity) at different location of the sample; it is possible that samples would not have a perfectly uniform fictive temperature even after an extended heat-treatment and quenching. Normally the best way to have uniform T_f within our samples should be to cut the glass sample into small pieces with nearly uniform composition and use them to obtain the calibration curves. However, such a study has never been reported because 1/ it is impossible to cut a highly Ge-doped preform rod into slices without breaking it due to the high level of stress, and 2/ this procedure is time and preforms consuming. But heating the fiber, drawn from the same perform, during a long time enough at a temperature T and next using our calibration curves yields a completely uniform T_f profile around T. This gives some confidence in our calibration curves.

Next, two main hypotheses (not exclusive) can be put forward to explain such observation. One explanation is the influence of the stress distribution on our measurements resulting in incorrect calibration curves since the stresses are different in the capillaries preform (used for calibration) and in fibers (used for measurements).

As it is well known, the IR reflection band of silica structural band near 1120cm^{-1}, which corresponds to the IR absorption band or Raman band at 1050cm^{-1}, shifts towards higher wavenumber under tensile stress and to lower wavenumber under compressive stress (Tomozawa, Lee et al. 1998; Tomozawa, Hong et al. 2004). However, the opposite trend has also been observed earlier for silica fibers, this artifact was caused by a surface corrosion layer (Tomozawa, Lee et al. 1998). Therefore, we have etched our samples just before FTIR experiments to remove this layer.

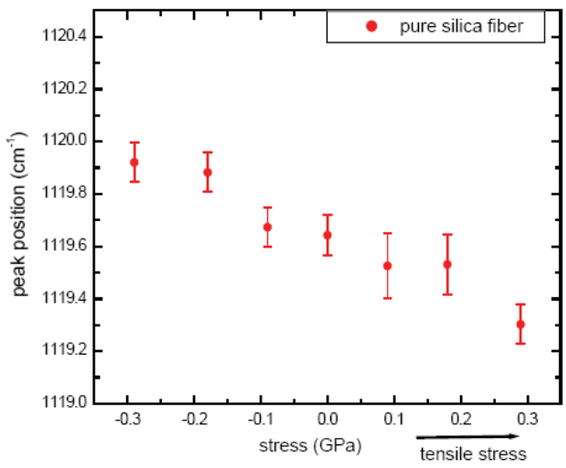

Fig. 19. Evolution of the 1120 cm^{-1} peak position according to the stress in pure silica core fiber (PSCF) (Hong 2003). Fiber was SMF made by MCVD process.

For example, MCVD GeO_2-doped core/SiO_2 cladding fiber was found to have an axial compressive stress in the inner cladding while tensile stress in the core, tube and outer-cladding (Limberger 2002). Furthermore, the higher the Ge-content, the higher the tensile stress in the core (Limberger 2002). Notice that this tensile stress would shift the peak to lower wavenumbers (Devine 1993; Tomozawa, Lee et al. 1998; Tomozawa, Hong et al. 2004), which is opposite to the observed trend.
Typically, the stress values recorded in optical fibers are around ± 100 MPa within the core (depending on the drawing tension and chemical composition) and less than 20 MPa in the tube or in the outer-cladding. Thus, the maximum compressive or tensile stress within the core of optical fibers is estimated to be in the range of –50 MPa and +100 MPa respectively in the axial direction.
The effect of residual stress on the IR peak wavenumber has been also investigated by Hong et al (Hong 2003). This is illustrated in Fig. 19 for a pure silica core fiber (PSCF). It is shown that the maximum elastic stress-induced shift of the 1120cm^{-1} band (or the equivalent one in Raman) was around 0.6 cm^{-1}/GPa (Tomozawa, Lee et al. 1998; Tomozawa, Hong et al. 2004). Thus, a -100 MPa uniaxial compressive stress is estimated to produce a peak shift < 0.1 cm^{-1}, which is much smaller than the observed peak shift attributed to the fictive temperature change. On the other hand, this value corresponds to our experimental error. **Therefore, the effect of the residual stress commonly found in optical fibers on the IR peak wavenumber is expected to have no measurable influence on our measurements.**

Another possibility is an inelastic strain within MMF cross section i.e. glass deformations that are not accompanied by the generation of stress. The inelastic strain is caused by the large temperature changes during fiber-drawing that freeze-in the relaxation contribution of the elastic properties (i.e. compressibility and shear compliance). It was reported that these inelastic contributions are frozen to their respective values at the glass fictive temperature (Dürr 2005). The inelastic strains mainly occur in the fiber region of highest viscosity which is, in general, the fiber cladding. It is possible that inelastic strain within outer-cladding does not allow the structural relaxation of the fiber core. **Thus, when the core changes from the supercooled liquid to the glass state, it is constrained by the cladding and cannot change its volume freely. This might produce a higher fictive temperature state in the core when compared with unconstrained cooling.**
This is in agreement with Ref. (Kim and Tomozawa 2001) where some "anomalies" were observed. Indeed, the Ge-doped silica glass used for the core had a higher viscosity, when compared to F-doped inner-cladding. When the fibers are produced at a given cooling rate, the glass with higher viscosity should have a higher T_f. Therefore, the Ge-doped core T_f was expected to exceed that of the F-doped inner cladding but we observe the opposite situation. Kim et al. (Kim and Tomozawa 2001; Kim, Tomozawa et al. 2001) suggested that when the inner cladding changes from a supercooled liquid to a glass state, the inner cladding is constrained by two rigid glasses (Ge-doped core and pure silica outer-cladding) on both sides, and then this could produce a higher T_f.

T_f vs densification effect:
In general, the fictive temperature increase is accompanied by small densification of glass structures. This volume change can be estimated from T_f changes. In this view, we will use the known relationship between fictive temperature and specific volume (density) for silica glass (Bruckner 1971) as shown in Fig. 20. The obtained relationship, below 1400°C, between

volume and T_f for type III silica glass is V (cm^3/g) = 0.4556 - $1.0937.10^{-6}$.T(°C), with R^2 = 0.99. This implies that for a 100°C T_f increases, this corresponds to roughly 10^{-4} relative volume change. On the other hand we can also deduce the impact of this small densification effect on the refractive index profile. Indeed, Arndt and Stoffler [27] have reported that the refractive index of silica glasses (at a constant OH content) increases with density for type III silica glass. Next, Hong et al. (Hong 2003) have extracted these data and drawn a regression line which is n = 1.8528 - 0.8683.V (cm^3/g) with R^2 = 0.96. Finally, the expected increase of refractive index (either at the fiber edges or in the fiber core) due to this densification effect was of the order of 10^{-4}.

On the other hand, it should be pointed out that the densification and refractive index changes estimated within the fiber core would be the maximum values to be expected from T_f changes. Indeed, the densification estimated would be realized only if the sample material can change its volume freely upon the T_f change. In the present sample, the Ge-doped fiber core cannot change its volume freely, constrained by the surrounding cladding. Therefore, the full densification expected by the fictive temperature increase may not occur. Furthermore, the impact of this densification effect (if occurs) on the fiber index profile remains quite negligible since it corresponds to less than 1% of the core/cladding index difference.

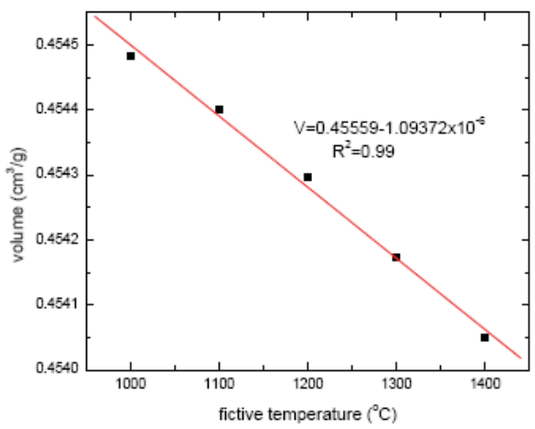

Fig. 20. Relationship between fictive temperature and specific volume (density) for bulk silica glass (Bruckner 1971; Hong 2003).

6. Applications 2: How to reduce T_f and thus Rayleigh scattering loss

Figure 21 shows the relationship between the Rayleigh scattering coefficient R and T_f. The solid and dotted lines show the relationships of pure and GeO_2-doped silica glass, respectively. The four circles and shaded areas represent the results for preforms and optical fibers, respectively. As shown in Fig. 21, the rapid cooling (without specific optimization) during the drawing process results in fiber T_f, which is at least 400°C higher than that measured in bulk samples. Thus, by lowering T_f, there is still a large possibility of reducing the Rayleigh scattering loss in optical fibers. These results strongly suggest that we should use the Rayleigh scattering coefficient of glass preforms to estimate the "intrinsic loss" or "minimum loss". With this definition, the intrinsic loss of each fiber is independent of its

drawing condition. Therefore, we will be able to consider the intrinsic loss as a practical target for loss reduction.

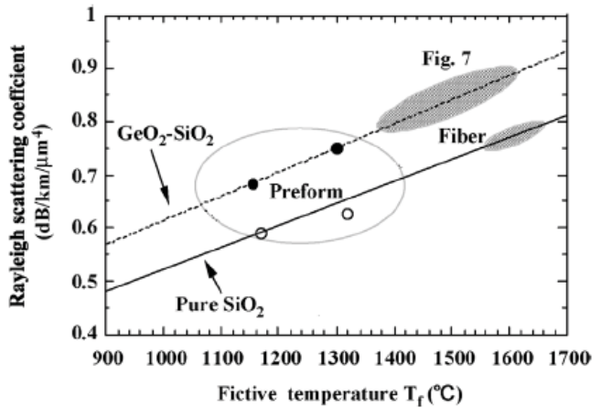

Fig. 21. Relationship between the R value and T_f. The four circles and shaded areas represent the results for preforms and optical fibers, respectively. Extracted from Ref. (Tsujikawa, Tajima et al. 2005).

In the literature, two main approaches have been practiced to reduce R via a reduction of T_f, namely one can optimize the core and/or cladding chemical compositions (Tajima, Ohashi et al. 1992; Lines 1994; Saito and Ikushima 1998; Saito, Kakiuchida et al. 1998; Tsujikawa, Tajima et al. 2000; Saito and Ikushima 2002; Saito, Yamaguchi et al. 2004), or optimize the thermal conditions of the fiber drawing (Todoroki and Sakaguchi 1997; Sakaguchi and Todoroki 1998; Sakaguchi 2000; Tsujikawa, Tajima et al. 2000; Tsujikawa, Tajima et al. 2005) against T_f. Physically, using these methods, the idea is to play with the structural relaxation time (e.g. τ becomes shorter). This should result in lower T_f and thus lower Rayleigh scattering coefficient R_ρ due to density fluctuations.

6.1 Optimization of the thermal conditions used for the fiber drawing

One possibility to reduce T_f as much as possible is to accelerate the structural relaxation by optimizing the fiber drawing process. In ref. (Hong 2003), Hong et al. study the influence of the drawing parameters (drawing tension, drawing speed) on the fictive temperature. The fiber composition was similar to commercial optical fibers (i.e. the core is 5.7 wt% of GeO_2). The fibers were produced under different process conditions such as cooling rates, drawing speed and tension force. Fiber samples were prepared following the blaze polished method, and the IR peak wavenumbers were then measured as a function of the fiber radius, as described in section III.B. Based on the calibration curves obtained in section IV, the fictive temperatures of fibers can be estimated.

6.1.1 Influence of drawing speed

(Hong 2003) has measured the fictive temperatures of three SMFs (made by MCVD) drawn at different speeds (between 400 m/min and 1000 m/min) and a constant tension force (30g). IR measurements were monitored on the fiber cross-section. The changes of fictive temperature are shown in Figure 22.

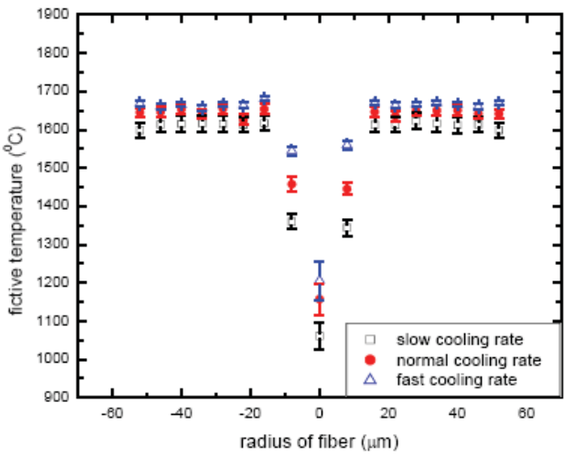

Fig. 22. T_f profile for 3 MCVD SMFs made with different drawing speeds. Extracted from Ref. (Hong 2003).

These measurements clearly show that the fictive temperature of the outer cladding is larger than that of the inner cladding, which is even larger than that of the core. The fictive temperatures of core, inner cladding and outer cladding at low drawing speed (drawing speed around 400m/min) are around ~1150 °C, ~1450 °C and ~1650 °C, respectively.
The fictive temperatures of both the core and the inner-cladding were higher at a higher drawing speed, while the fictive temperature of the outer-cladding was slightly higher at a higher drawing speed. The obtained fictive temperature changes are consistent with what was expected: as drawing speed increases, the cooling rate increases, yielding higher fictive temperatures.

6.1.2 Influence of drawing tension

The fictive temperatures of optical fibers made under different tension forces were also estimated. Holding the drawing speeds constant (400 m/min), two different drawing tensions were tested (30 g and 120g) (Hong 2003). Figure 23 shows the changes of fictive temperature with different tension forces. As tensile forces increased, the fictive temperatures decreased in both the core and the inner cladding. The T_f of the core decreases from 1280°C down to 1220°C (high tension). This leads to an increase of the Rayleigh density fluctuation coefficient i.e. $\Delta R_\rho \approx +$ 5-10%.

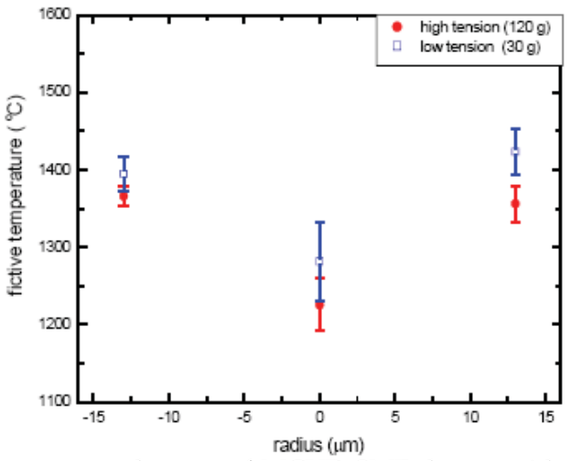

Fig. 23. The fictive temperature changes of MCVD SMF drawn with different tensions as a function of the fiber radius. Extracted from Ref. (Hong 2003).

6.1.3 Influence of drawing temperature

Figure 24 shows the relationship between the R value of various optical fibers and their drawing temperature T_d. The lowest R value, 0.66 for P_2O_5-doped silica core fiber, results from the low T_f value, because P_2O_5 doping effectively reduces the glass viscosity. On the other hand, the R value of the GeO_2-doped silica core fiber decreased linearly as the Td value decreased. This proves that the R value of optical fibers can be controlled via T_f by adjusting the drawing temperature and speed (Tajima 1998; Tsujikawa, Tajima et al. 2000; Tsujikawa, Tajima et al. 2005) i.e. by drawing them slowly at a lower temperature. However, since relaxation time τ increases exponentially with decreasing T_d, the cooling should become exponentially slower for decreasing T_f, which makes it difficult to reduce optical loss. In addition, this usually results in higher stress level (Limberger 2002). The optimum thermal conditions have already been analyzed theoretically and reported in Refs (Sakaguchi and Todoroki 1999; Sakaguchi 2000; Saito, Yamaguchi et al. 2003).

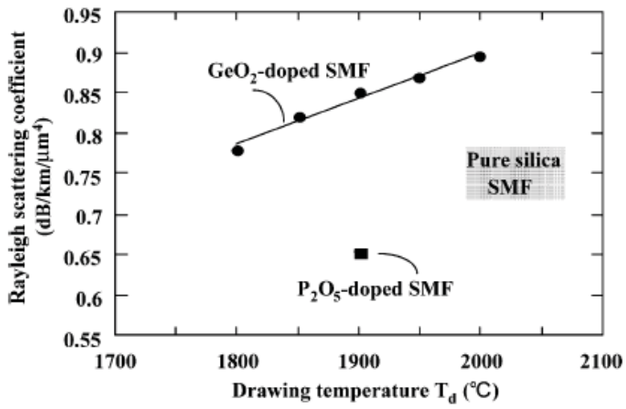

Fig. 24. Relationship between the *R* value of the test fibers and their drawing temperature T_d. Fibers were SMF made by VAD process. Extracted from Ref. (Tsujikawa, Tajima et al. 2005)

Figure 25 shows the intrinsic losses (multiphonon absorption and Rayleigh scattering) of silica-based fibers re-evaluated by using the R value of the preforms shown in Fig. 21. The theoretical loss of GeO_2-doped silica glass, which corresponds to conventional SMF, is 0.130 dB/km at 1.55 μm. The values for pure and slightly P_2O_5-doped silica glasses are 0.115 and 0.095 dB/km, respectively. These values are 0.03–0.05 dB/km lower than the lowest experimental value of 0.1484 dB/km for pure silica core SMF (Nagayama, Kakui et al. 2002). Knowing that the multiphonon absorption results in 0.01 to 0.02dB/km at 1.55μm. Thus, there is still a large possibility of reducing the Rayleigh scattering loss in such optical fibers (0.01 to 0.04dB/km).

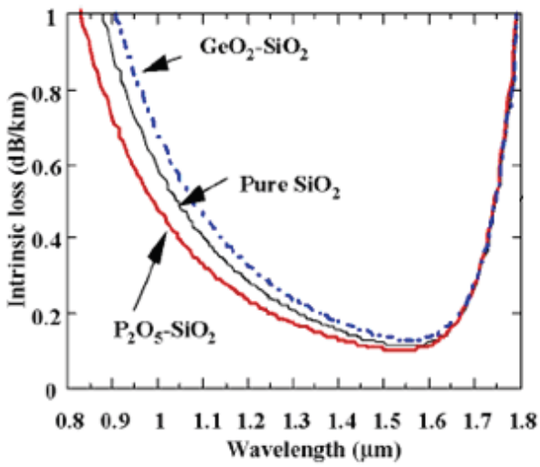

Fig. 25. Intrinsic losses of silica-based fibers re-evaluated by using the R values measured in preforms. Extracted from Ref. (Tsujikawa, Tajima et al. 2005).

6.1.4 Playing with the cooling profile: effect of optimized drawing conditions

Figure 26 shows the relative change in fictive temperature distribution on the cross section of the "reference" (not optimized drawing conditions) MMF together with that of P2 fiber (drawn in optimized conditions). The absolute error bars in fictive temperature have been estimated from those in wavenumbers and calibration curves. T_f along the entire cross-section for the "reference" P1 fiber varies with the radial position and was everywhere higher than that measured in the optimized P2 fiber. Firstly, the estimated fictive temperatures of the P1 fiber at the near-surface region are ≈ 200°C higher than in the internal part of the outer cladding of the fiber. This is presumably due to a faster cooling rate at the fiber surface. Secondly, there is an increase (≈ 150°C) of the fictive temperature from the tube towards the center of the core. In contrast, for the optimized P2 fiber, the fictive temperatures were relatively constant within the whole optical fiber cross section. From our calculation, this approach can lead up to a 15% loss reduction at 850nm in such MMF.

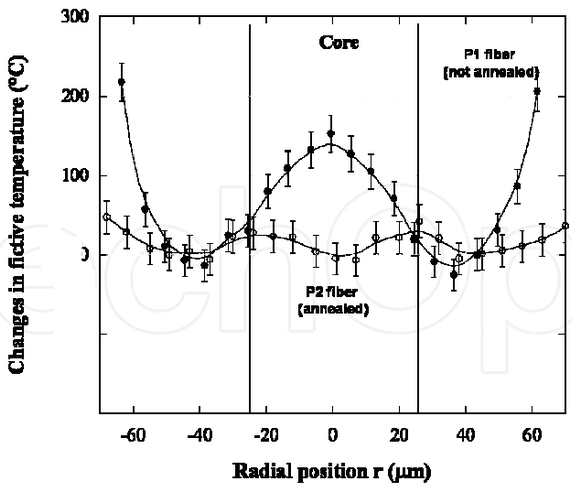

Fig. 26. Relative change in MMF fictive temperature as a function of the radial position for P1 (not optimized drawing conditions) and P2 (optimized drawing conditions) fibers. The solid lines are guides for eyes. Fibers were MMF made by PCVD process.

6.1.5 Playing with the cooling profile: Annealing furnace

Another possibility is to favor the structural relaxation during the fiber drawing process. To do that, annealing furnaces can be mounted on the drawing towers. The temperature of the furnace can be kept constant at an annealing temperature T_a, or it follows a gradient profile (Kakiuchida, Sekiya et al. ; Sakaguchi 2000; Tsujikawa, Tajima et al. 2005; Lancry, Flammer et al. 2007; Martinet, Martinez et al. 2008). ***T_a profile, t_a (annealing time) and L (furnace length) should be optimized to minimize T_f by taking into account the thermal history (initial T_f).***

Figure 27 shows an example of the impact of the thermal cooling profile on the Rayleigh scattering level. In this case, the annealing furnace is 3m long and the drawing speed is either 600m/min ("normal" drawing speed) or 30m/min (slow drawing speed). The annealing furnace was set to 1400°C. Keeping the drawing speed relatively high (600m/min), it is possible to decrease the fictive temperature down to 1130°C, leading to a reduction of the Rayleigh scattering coefficient by 10% at least (Sakaguchi 2000). From a practical point of view, we can conclude that the annealing furnace allows to reduce efficiently T_f (and thus the Rayleigh scattering loss) within the fiber core.

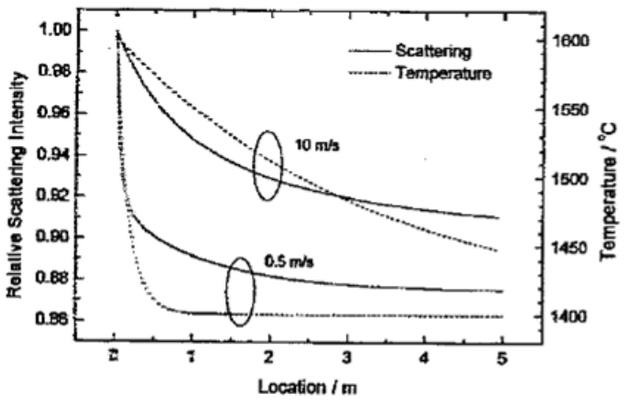

Fig. 27. Variations of the relative Rayleigh scattering loss and the fiber's temperature as a function of the length of the annealing furnace (set to 1400°C) mounted on the draw tower. Fibers were SMFs made by VAD process. Extracted from Ref. (Sakaguchi 2000).

To conclude this part, it is thus possible to optimize the cooling profile to minimize T_f by taking into account the thermal history Furthermore, as the dopants can change the relaxation time, it follows that the chemical composition of both core and cladding has to be taken into account before performing the thermal optimization. This is the main objective of the next sub-section.

6.2 Optimizing the optical fiber chemical composition:

6.2.1 Playing with the core chemical composition

Instead of playing directly on the cooling profile, another possibility is to accelerate the relaxation time τ_{core} of the core for lowering T_f (and thus Rayleigh loss). Indeed, the relaxation time τ_{core} of the core can be shortened by an appropriate doping of the core and/or cladding (Kakiuchida, Sekiya et al. ; Tajima, Ohashi et al. 1992; Lines 1994; Saito and Ikushima 1998; Saito, Kakiuchida et al. 1998; Tsujikawa, Tajima et al. 2000; Kakiuchida, Saito et al. 2002; Saito and Ikushima 2002; Kakiuchida, Saito et al. 2003; Saito, Yamaguchi et al. 2004). Indeed, small compositional variations can have a huge impact on the glass viscosity and thermal expansion coefficient and thus on accessible drawing temperature, stress distribution (mainly due to thermal expansion coefficient mismatch) and thus in the resulting fictive temperature. This path has been extensively studied by Sumitomo and NTT to reduce the SMF fictive temperature efficiently. This implies the possibility of further reduction of the Rayleigh scattering by heat treatment for a shorter duration at lower temperature.

For example, it should be pointed out that F-doping (Kakiuchida, Saito et al. 2002; Saito and Ikushima 2002; Kakiuchida, Saito et al. 2003; Saito, Yamaguchi et al. 2004) or Cl-doping (Kakiuchida, Sekiya et al. ; Kakiuchida, Saito et al. 2003) of the core accelerates the reduction of the T_f in the core (with optimized thermal conditions). This is illustrated in Fig. 28 where the Rayleigh scattering coefficient is drawn according to the fictive temperature for various F content (Kakiuchida, Saito et al. 2002). It is shown that it is possible to achieve lower T_f but at the expense of higher Rayleigh scattering loss due to concentration fluctuations. Table 6 summarizes the most important results about this method.

Methods	Comments
Core	
Ge-doped **0 – 30 mol %**	• ↑ Ge ⇒ lower viscosity ⇒ lower τ ⇒ lower T_f • ↑ Ge ⇒ lower Rayleigh loss sensibility to cooling conditions • ↑ Ge ⇒ concentration fluctuation ⇒ higher R_c (linear relationship)
P-doped **0 – 1 mol %**	• ↑ P ⇒ lower viscosity ⇒ lower τ ⇒ lower T_f • Lower Rayleigh loss due to lower density fluctuation R_ρ • Concentration fluctuations Rc remain low because P concentration remains small
F-doped **0 - 7 mol%**	• ↑ F ⇒ lower viscosity ⇒ lower τ ⇒ lower T_f • ↑ F ⇒ concentration fluctuation ⇒ higher R_c (linear relationship) • T_f and density fluctuation R_ρ independent of F content
Cl-doped **0 - 2 mol%**	• Rayleigh loss (both R_c and R_ρ) independent of Cl content • Cl accelerates the structural relaxation of the core and T_f can thus be reduce by heat treatment for a shorter duration with higher Cl concentration
Cladding	
F-doped **0 - 4 mol%**	• Lower T_f and Rayleigh loss in the fiber core • Slight increase of the R_c in the cladding • F accelerates the structural relaxation (smaller τ) (and thus volume change) 1) if $\tau_{cladd} > \tau_{core}$: Suppresses the structural relaxation in the core 2) if $\tau_{cladd} < \tau_{core}$: Accelerates the structural relaxation in the core
Na-doped **< 100 ppm**	• Na introduction in outer-cladding accelerates the structural relaxation of the core • Lower T_f and thus lower Rayleigh loss in the core • But higher Hydrogen sensitivity

Table 6. Optimizing the optical fiber chemical composition in order to decrease the Rayleigh scattering loss in silica-based optical fibers.

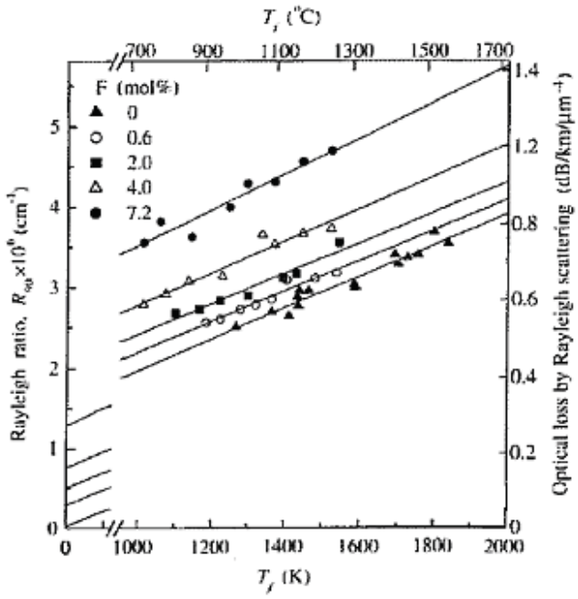

Fig. 28. Relationship between the Rayleigh scattering loss and the fictive temperature for F-doped silica core. The solid lines are linear fitting. Fibers were SMF made by VAD process. Extracted from Ref. (Kakiuchida, Saito et al. 2002).

6.2.2 Playing with the cladding chemical composition

However, a problem with core doping is that Rayleigh scattering due to concentration fluctuations (R_c) generally increases with increasing dopant concentration contrarily to the reduction of density fluctuation contribution R_ρ. To avoid this problem, small compositional variations (typ. below 1 w%) have been proposed and especially within the outer part (i.e. cladding, tube, outer-cladding). Indeed, it has been observed that τ_{core} is strongly affected by the structural relaxation of the cladding (Saito, Yamaguchi et al. 2004). ***Basically, it has been suggested that when $\tau_{clad} > \tau_{core}$, the structural relaxation in the core is suppressed. Indeed, in this temperature range, the core is willing to increase its specific volume but cannot change its volume freely due to the cladding. The effective τ_{core} is thus larger than expected in unconstrained samples. At the opposite, if $\tau_{clad} < \tau_{core}$, the structural relaxation in the core becomes easier***. In the last case, the idea is to increase the structural relaxation time of the core by an appropriate doping of the outer-cladding. For example, it should be pointed out that F-doping (Saito, Yamaguchi et al. 2004; Gonnet, Nouchi et al. 2007) or Na-doping (see below) of the cladding favors the reduction of T_f in the core (with optimized thermal conditions) while the effect of Al should be the opposite.

A recent example has been developed at Draka Communications (Gonnet, Nouchi et al. 2007). The main idea was to introduce small compositional variations in the fiber outer-cladding. For example, the effect of doping MMF's outer-cladding with Na, K and F on the core T_f has been investigated. Such measurements are reported in Table 7. As it can be seen, the Na-doped MMF core has a T_f which is 100°C lower than the others. For going further in this direction, various Na contents were introduced within the outer-cladding. In the investigated range of Na content, the higher is the Na content in the outer-cladding, the lower is the T_f within the core. However, this method should not be pushed too far, as it has been shown that too large amounts of alkalines could lead to a larger H_2-sensitivity of fibers (Ogai, Iino et al. 1987). If possible, it is thus important to avoid Na migration towards the fiber core by choosing appropriate drawing conditions.

Fiber label	P1	P2	P3	P4
Outer-cladding doping	Pristine	F	K	Na
ΔT_f (°C)	Ref	-50°C	-80°C	- 100°C

Table 7. Changes in T_f for MMFs with different outer-cladding chemical compositions.

7. Conclusion

Infrared spectroscopy was demonstrated to be an efficient tool for determining the fictive temperatures of bulk silica glass and silica-based optical fibers. The calibration curves between IR wavenumbers and fictive temperature were obtained by monitoring the peak position of the fundamental structural band (asymmetric vibration band).

It has been shown that two approaches are efficient for reducing the Rayleigh scattering coefficient, namely optimization of the optical fiber core and/or cladding composition and optimization of the thermal conditions used for the fiber drawing (e.g. drawing temperature drawing speed, drawing tension, cooling profile). A combination of these approaches is promising in terms of achieving further the loss reduction for silica-based optical fibers.

8. References

Agarwal, A., K. Davis, et al. (1995). "A simple IR spectroscopic method for determining fictive temperature of silica glasses." Journal of non-crystalline solids **185**(1-2): 191-198.

Agarwal, A. and M. Tomozawa (1995). "Determination of fictive temperature of soda-lime silicate glass." Journal of the American Ceramic Society **78**(3): 827-829.

Agarwal, A. and M. Tomozawa (1997). "Correlation of silica glass properties with the infrared spectra." J. Non-Cryst. Solids **209**(1): 166-174.

Almeida, R. (1992). "Detection of LO modes in glass by infrared reflection spectroscopy at oblique incidence." Physical review. B, Condensed matter **45**(1): 161.

Bachmann, P., W. Hermann, et al. (1987). "Stress in optical waveguides. 2: Fibers." Applied optics **26**(7): 1175-1182.

Bell, R., N. Bird, et al. (1968). "The vibrational spectra of vitreous silica, germania and beryllium fluoride." Journal of Physics C Solid State Physics **1**(2): 299-303.

Bruckner, R. (1970). "Properties and structure of vitreous silica. I." J. Non-Cryst. Solids **5**(2): 123–175.

Bruckner, R. (1971). "Metastable equilibrium density of hydroxyl-free synthetic vitreous silica." J. Non-Cryst. Solids **5**(4).

Champagnon, B., C. Chemarin, et al. (1998). "Fictive temperature and medium range order in silicate glasses: a relationship between heat capacity and boson peak." Philosophical Magazine Part B **77**(2): 663-669.

Dalle, C. Contribution à l'étude des mécanismes liés à la photosensibilité de type I et de type IIA des verres de silice par Spectroscopie Infrarouge et Microscopie Electronique en Transmission.

Devine, R. (1993). "Ion implantation- and radiation-induced structural modifications in amorphous SiO? 2 ?" Journal of non-crystalline solids **152**(1): 50-58.

Dürr, F. (2005). Laser-induced stress changes in optical fibers, Ph. D. dissertation, Swiss Federal Inst. Technol.(EPFL), Lausanne, Switzerland.

Fraser, D. (1968). "Factors influencing the acoustic properties of vitreous silica." Journal of Applied Physics **39**: 5868.

Galeener, F. (1979). "Band limits and the vibrational spectra of tetrahedral glasses." Physical Review B **19**(8): 4292-4297.

Gonnet, C., P. Nouchi, et al. (2007). Method for manufacturing an optical fiber preform, optical fiber preform and optical fiber, EP Patent 1,813,581.

Helander, P. (2004). "Measurement of fictive temperature of silica glass optical fibers." Journal of Materials Science **39**(11): 3799-3800.

Hong, J. (2003). FTIR investigation of amorphous silica fibers and nano-size particles Ph. D, dissertation Rensselaer Polytechnic Institute, Troy, NY.

Hong, J., S. Ryu, et al. (2004). "Investigation of structural change caused by UV irradiation of hydrogen-loaded Ge-doped core fiber." Journal of non-crystalline solids **349**: 148-155.

Hosono, H., Y. Ikuta, et al. (2001). "Physical disorder and optical properties in the vacuum ultraviolet region of amorphous SiO (2)." Physical review letters **87**(17): 175501.

Irven, J., A. Harrison, et al. (1981). "Long wavelength performance of optical fibres co-doped with fluorine." Electronics Letters **17**(1): 3-5.

Kakiuchida, H., K. Saito, et al. (2003). Effects of halogen doping on structure of silica glass as a photonic material.

Kakiuchida, H., K. Saito, et al. (2002). Rayleigh scattering in fluorine-doped silica glass.

Kakiuchida, H., E. Sekiya, et al. "Effect of chlorine on Rayleigh scattering reduction in silica glass." Jpn. J. Appl. Phys **42**(12B pt 2).

Kao, C. (1983). "Optical Fiber Systems: Technology, Design, and Application."

Kim, D. and M. Tomozawa (2001). "Fictive temperature of silica glass optical fibers–re-examination." Journal of non-crystalline solids **286**(1-2): 132-138.

Kim, D., M. Tomozawa, et al. (2001). "Fictive temperature measurement of single-mode optical-fiber core and cladding." Journal of lightwave technology **19**(8): 1155.

Koike, A., S. Ryu, et al. (2005). "Adequacy test of the fictive temperatures of silica glasses determined by IR spectroscopy." Journal of non-crystalline solids **351**(52-54): 3797-3803.

Lancry, M., I. Flammer, et al. (2007). "Fictive-Temperature Mapping in Highly Ge-Doped Multimode Optical Fibers." Journal of lightwave technology **25**(5): 1198-1205.

Lancry, M., I. Flammer, et al. (2007). "Fictive temperature distribution in highly Ge-doped multimode optical fibers." Journal of non-crystalline solids **353**(5-7): 473-476.

Le Parc, R. (2002). Diffusion de rayonnements et relaxation structurale dans les verres de silice et les préformes de fibres optiques Ph. D, dissertation Univ. Claude BernardLyonFrance.

Limberger, H. (2002). POWAG'2002, White Nights' Summer School on Photosensitivity in Optical Waveguides and Glasses, St. Petersburg, Russia.

Lines, M. (1984). "Scattering losses in optic fiber materials. I. A new parametrization." Journal of Applied Physics **55**: 4052.

Lines, M. (1994). "Can the minimum attenuation of fused silica be significantly reduced by small compositional variations? I. Alkali metal dopants." Journal of Non Crystalline Solids **171**(3): 209-218.

Martinet, C., V. Martinez, et al. (2008). "Radial distribution of the fictive temperature in pure silica optical fibers by micro-Raman spectroscopy." Journal of Applied Physics **103**: 083506.

Martinez, L. and C. Angell (2002). "Chemical order lifetimes in liquids, and a second fictive temperature for glassformers." Physica A: Statistical Mechanics and its Applications **314**(1-4): 548-559.

Matthijsse, P., F. Gooijer, et al. (2007). Fluorine-Doped Optical Fiber, Google Patents.

Miller, S. and A. Chynoweth (1979). "Optical fiber telecommunications." New York: Academic Press, 1979, edited by Miller, Stewart E.; Chynoweth, Alan G.

Nagayama, K., M. Kakui, et al. (2002). "Ultra-low-loss (0.1484 dB/km) pure silica core fibre and extensionof transmission distance." Electronics Letters **38**(20): 1168-1169.

Ogai, M., A. Iino, et al. (1987). "Behavior of alkali impurities and their adverse effect on germania-doped silica fibers." Lightwave Technology, Journal of **5**(9): 1214-1218.

Othonos, A. (1997). "Fiber Bragg Gratings." Review of scientific instruments **68**: 4309.

Peng, Y., A. Agarwal, et al. (1997). "Radial distribution of fictive temperatures in silica optical fibers." J. Non-Cryst. Solids **217**(2): 272-277.

Pinnow, D., S. Candau, et al. (1968). "Brillouin scattering: viscoelastic measurements in liquids." The Journal of the Acoustical Society of America **43**: 131.

Pinnow, D., S. Candau, et al. (1968). "Rayleigh Scattering: Orientational Relaxation in Liquids." The Journal of chemical physics **49**: 347.

Regnier, E., G. Kuyt, et al. (2008). Radiation-resistant fluorine doped optical fiber, EP Patent 1,876,150.
Regnier, E., B. Poumellec, et al. (2005). "Infrared optical properties of highly P doped silica fibres: a spectroscopic study." Glass Technology **46**(2): 99-102.
Saito, K. and A. Ikushima (1998). "Structural relaxation enhanced by Cl ions in silica glass." Applied Physics Letters **73**: 1209.
Saito, K. and A. Ikushima (2002). "Effects of fluorine on structure, structural relaxation, and absorption edge in silica glass." Journal of Applied Physics **91**: 4886.
Saito, K., H. Kakiuchida, et al. (1998). "Light-scattering study of the glass transition in silica, with practical implications." Journal of Applied Physics **84**: 3107.
Saito, K., M. Yamaguchi, et al. (2004). "Approach for reducing the Rayleigh scattering loss in optical fibers." Journal of Applied Physics **95**: 1733.
Saito, K., M. Yamaguchi, et al. (2003). "Limit of the Rayleigh scattering loss in silica fiber." Applied Physics Letters **83**: 5175.
Sakaguchi, S. (2000). "Relaxation of Rayleigh scattering in silica core optical fiber by heat treatment." Electronics and Communications in Japan (Part II: Electronics) **83**(12).
Sakaguchi, S. and S. Todoroki (1998). "Rayleigh scattering of silica core optical fiber after heat treatment." Applied optics **37**: 7708-7711.
Sakaguchi, S. and S. Todoroki (1999). "Viscosity of silica core optical fiber." Journal of non-crystalline solids **244**(2-3): 232-237.
SHACKELFORD, J., J. MASARYK, et al. (1970). "Water Content, Fictive Temperature, and Density Relations for Fused Silica." Journal of the American Ceramic Society **53**(7): 417-417.
Simmons-Potter, K., B. Potter Jr, et al. (1996). "Novel process for the production of large, stable photosensitivity in glass films." Applied Physics Letters **68**: 2011.
Tajima, K. (1998). Low-loss optical fibers realized by reduction of Rayleighscattering loss.
Tajima, K., M. Ohashi, et al. (1992). "Low Rayleigh scatteringP 2 O 5-F-SiO 2 glasses." Lightwave Technology, Journal of **10**(11): 1532-1535.
Todoroki, S. and S. Sakaguchi (1997). "Rayleigh scattering and fictive temperature in VAD silica glass with heat treatment." Nippon seramikkusu kyokai gakujutsu ronbunshi **105**(5): 377-380.
Tomozawa, M., J. Hong, et al. (2004). "IR investigation of the structure of silica glass fibers." GLASS SCIENCE AND TECHNOLOGY-FRANKFURT AM MAIN- **75**: 262-276.
Tomozawa, M., Y. Lee, et al. (1998). "Effect of uniaxial stresses on silica glass structure investigated by IR spectroscopy." J. Non-Cryst. Solids **242**(2): 104-109.
Tsujikawa, K., K. Tajima, et al. (2000). "Rayleigh scattering reduction method for silica-based optical fiber." Journal of lightwave technology **18**(11): 1528.
Tsujikawa, K., K. Tajima, et al. (2005). "Intrinsic loss of optical fibers." Optical Fiber Technology **11**(4): 319-331.
Wissuchek, D., C. Ponader, et al. (1999). Analysis of residual stress in optical fiber.
Zarzycki, J. (1982). Glass and the Vitreous State (Les Verres et 1'Etat Vitreaux), Masson, Paris.

IntechOpen

Optical Fiber New Developments

Edited by Christophe Lethien

ISBN 978-953-7619-50-3

Hard cover, 586 pages

Publisher InTech

Published online 01, December, 2009

Published in print edition December, 2009

The optical fibre technology is one of the hop topics developed in the beginning of the 21th century and could substantially benefit applications dealing with lighting, sensing and communication systems. Many improvements have been made in the past years to reduce the fibre attenuation and to improve the fibre performance. Nowadays, new applications have been developed over the scientific community and this book fits this paradigm. It summarizes the current status of know-how in optical fibre applications and represents a further source of information dealing with two main topics: the development of fibre optics sensors, and the application of optical fibre for telecommunication systems.

How to reference

In order to correctly reference this scholarly work, feel free to copy and paste the following:

Matthieu Lancry, Elise Regnier and Bertrand Poumellec (2009). Fictive Temperature Measurements in Silicabased Optical Fibers and Its Application to Rayleigh Loss Reduction, Optical Fiber New Developments, Christophe Lethien (Ed.), ISBN: 978-953-7619-50-3, InTech, Available from: http://www.intechopen.com/books/optical-fiber-new-developments/fictive-temperature-measurements-in-silicabased-optical-fibers-and-its-application-to-rayleigh-loss-

INTECH
open science | open minds

InTech Europe
University Campus STeP Ri
Slavka Krautzeka 83/A
51000 Rijeka, Croatia
Phone: +385 (51) 770 447
Fax: +385 (51) 686 166
www.intechopen.com

InTech China
Unit 405, Office Block, Hotel Equatorial Shanghai
No.65, Yan An Road (West), Shanghai, 200040, China
中国上海市延安西路65号上海国际贵都大饭店办公楼405单元
Phone: +86-21-62489820
Fax: +86-21-62489821

IntechOpen